J. Fluid Mech. (1998), *vol.* 363, *pp.* 25–56. Printed in the United Kingdom

An experimental study of the motion of concentrated suspensions in two-dimensional channel flow. Part 1. Monodisperse systems

By M. K. LYON† AND L. G. LEAL

University of California, Santa Barbara, Department of Chemical Engineering, Santa Barbara, CA 93106, USA

(Received 13 November 1997 and in revised form 8 December 1997)

A modified laser-Doppler velocimetry method is utilized to measure fully developed particle velocity and concentration profiles, as well as the mean-square amplitudes of velocity fluctuations (i.e. one component of the so-called particle temperature), for concentrated monodisperse suspensions across the narrow gap of a rectangular channel. A stable index-of-refraction match of the suspending and particulate phases in conjunction with short-focal-length focusing optics has enabled data acquisition up to particle volume fractions of 0.50. In general, the particle concentration distributions possess a maximum near the channel centreline and a minimum at the channel walls. Coupled to these concentration distributions were blunted velocity profiles, and particle velocity fluctuation distributions that had a sharp maximum at gap positions approximately 80% of the way from the channel axis towards the walls. The particle velocity distributions were consistent with the absence of slip between particles and the suspending fluid.

The experimental data were compared with theoretical predictions from the diffusive flux model (Leighton & Acrivos 1987; Phillips *et al.* 1992), a model due to Mills & Snabre (1995), and the suspensions balance model (McTigue & Jenkins 1992; Nott & Brady 1994). The influence of bulk particle concentration, suspension volumetric flow rate, and ratio of channel gap width to particle diameter on the fully developed profiles was qualitatively consistent with the theoretical predictions from all three models. For the diffusive flux and suspension balance models, we used both literature values for model parameters, and values obtained from a best fit to our entire set of experimental data. Overall, the Mills & Snabre and suspension balance models were found to provide a better quantitative fit to the experimental data than the diffusive flux model.

1. Introduction

Over the past decade significant effort has been expended studying concentrated suspensions composed of neutrally buoyant, non-colloidal rigid spherical particles immersed in a viscous Newtonian fluid undergoing two-dimensional pressure-driven flow through circular and rectangular conduits (Averbakh *et al.* 1997; Chung 1980; Hampton *et al.* 1997; Hookham 1986; Koh 1991; Koh *et al.* 1994; Nott & Brady 1994; Sinton & Chow 1991). Of particular interest is the form of the fully developed particle velocity and concentration profiles. Qualitatively, it is known that a non-uniform particle concentration distribution develops within the conduit cross-section as a consequence of irreversible interactions between the particles during flow, which is then

† Present address: Department of Mechanical Engineering and Applied Mechanics, University of Michigan, Ann Arbor, MI 48109-2121, USA.

reflected in a velocity profile that is 'blunted' relative to the well-known parabolic shape for a homogeneous Newtonian fluid.

The first formal recognition of flow-induced concentration non-uniformities caused by particle interactions was due to Leighton & Acrivos (1987) who used them to explain transient stresses that were observed when a concentrated suspension was subjected to a simple Couette flow. Specifically, they attributed these transients in the suspension stress to the migration of particles caused by spatial gradients in the particle interaction frequency (or alternatively, against gradients in the local shear stress and particle concentration). From these arguments and simple dimensional analysis, Leighton & Acrivos derived diffusive flux expressions for the particulate phase, and demonstrated that these were consistent with the existence of a fully developed non-uniform particle concentration distribution for flow within a parallel wall channel. Although this result contradicted the uniform particle concentration profiles that had been reported by Karnis *et al.* (1966) for concentrated suspension flows within circular tubes, it has subsequently been pointed out that the inherent precision of the latter's tracer particle technique would not have allowed a non-uniform particle concentration distribution to be statistically distinguished from a uniform one (Hampton *et al.* 1997; Leighton 1985; Leighton & Acrivos 1987).

More recent experimental investigations of concentrated suspension flows through tubes and channels have attempted to quantify concentration and velocity profiles under fully developed conditions. A previous study from this lab utilized laser Doppler velocimetry (LDV) to measure both the velocity and concentration profiles of the suspended particles in a two-dimensional channel. These measurements demonstrated the existence of blunted velocity profiles that were independent of the suspension flow rate (Koh *et al.* 1994), but which became increasingly blunted as either the concentration of particles ϕ_{bulk} or the particle size relative to the channel dimension was increased (Koh *et al.* 1994; Hookham 1985). The particle concentration profiles were non-uniform with a maximum in the region of the channel centreline, which became more pronounced with increasing particle concentration (Koh *et al.* 1994; Hookham 1985). However, these studies were limited to particle concentrations of 30% or less by volume, which coincides with the lower limit at which Leighton & Acrivos observed 'shear-induced migration'. Furthermore, recent numerical results for the evolution of the velocity and concentration profiles suggest that many of these measurements did not occur far enough downstream from the conduit entrance for the concentration profiles to become fully developed (Hampton *et al.* 1997; Nott & Brady 1994, Phan-Thien & Fang 1996).

Measurements with higher particle concentrations have utilized suspensions with more stable refractive index matches combined with improved LDV technology, or implemented magnetic resonance imaging (MRI) (or nuclear magnetic resonance, NMR), which does not require the matching of the particles and suspending fluid optical properties. Until recently, these studies yielded quantitative data only for the velocity profile (Averbakh *et al.* 1997; Sinton & Chow 1991), while measured concentration distributions were at best qualitative (Sinton & Chow 1991). Moreover, the use of small relative particle sizes in these studies again suggests that these profiles were not fully developed.

Recently, Hampton *et al.* (1997) have reported fully developed suspending-fluid velocity and concentration profiles for suspension flows within a circular tube for $0.10 \leqslant \phi_{bulk} \leqslant 0.45$ and ratio of tube to particle radii, R_0/a, values of 16 and 39. For $\phi_{bulk} = 0.10$, the suspending-phase velocity and particulate-phase concentration profiles were parabolic and uniform, in agreement with the earlier results of Hookham (1985)

and Kowalewski (1980). However, for $\phi_{bulk} \geqslant 0.20$ the data showed blunted velocity profiles that were independent of the suspension flow rate, as well as non-uniform concentration distributions, in which a sharp maximum was measured in the region of the tube axis. The magnitude of the concentration maximum was found to increase as either R_0/a or the particle concentration increased.

A number of theoretical models have also been developed that can be used to calculate steady-state velocity and concentration profiles for two-dimensional flows of concentrated suspensions (Buyevich 1996; McTigue & Jenkins 1992; Leighton & Acrivos 1987; Mills & Snabre 1995; Phillips *et al.* 1992). In general, these models approximate the suspension rheology as a generalized Newtonian fluid with a concentration-dependent viscosity. These models differ, however, in their approach to calculating the particle concentration distribution. Generally, two approaches are utilized. The first is the aforementioned diffusive flux method of Leighton & Acrivos, which utilizes expressions for the flux of particles resulting from gradients in particle concentration and stress to write a conservation equation for the local particle concentration. Using the notation of Phillips *et al.* (1992), the fully developed particle concentration profile for two-dimensional channel flow can be determined iteratively by solving

$$\phi(x) = \phi_m \left[1 - \frac{\phi_m x}{k(1-\phi/\phi_m)^{\chi-1} + \phi_m x} \right], \tag{1}$$

where ϕ_m is the particle volume fraction at which the suspension viscosity diverges to infinity, x is the spatial variable across the channel gap, k is a constant that is determined from the total volume flux of particles through the channel cross-section, and χ is a measure of the relative magnitudes of the two aforementioned particle migration fluxes.

The second approach utilizes a particulate-phase momentum balance transverse to the direction of flow, along with recognition of a particle-phase normal stress that results from particle interactions, to obtain an equation for the particle concentration profile (Nott & Brady 1994; Buyevich 1996; McTigue & Jenkins 1992; Mills & Snabre 1995). At steady state, the governing equation is given by

$$\nabla \cdot \boldsymbol{\Pi} = 0, \tag{2}$$

where $\boldsymbol{\Pi}$ is the particle phase normal stress tensor. The form of $\boldsymbol{\Pi}$ is distinct for the various models of this class, with differences arising from the approach taken to eliminating the local nature of the diffusive flux model. Mills & Snabre (1995) deduced a form of $\boldsymbol{\Pi}$ by summing the single-particle time-averaged lubrication drag force over all particles within the plane of shear, and then assumed that the overall suspension stress is transmitted through a transient cluster of particles that spans the conduit cross-section. This yields a non-local normal particle stress of the form

$$\Pi_{xx} = \frac{-\phi}{1-\phi/\phi^*} \frac{Px^2}{2a}, \tag{3}$$

where P is an isotropic pressure term, and ϕ^* is defined in a manner analogous to ϕ_m. Although this model is applicable for the two-dimensional channel flow of interest, it should be emphasized that it is not applicable for inhomogeneous flows, such as an eccentric journal bearing, because it is not invariant to changes of reference frame.

The suspension balance model (McTigue & Jenkins 1992; Nott & Brady 1994) on the other hand argues that in order for the particulate normal stress to be non-local, it should depend upon the time average of the square of the particle velocity fluctuations (i.e. the so-called particle-based 'temperature' field) $T(x)$, rather than the local shear

rate $\dot{\gamma}$, because $T(x)$ takes into account the physical size of the particles. Using the notation of Nott & Brady (1994) the generalized form for $\boldsymbol{\Pi}$ is then given by

$$\boldsymbol{\Pi} = [\boldsymbol{\Pi}_0 + \mu(\phi)\, p(\phi)(w_t\, a^{-1} T^{1/2} + w_g\, \dot{\gamma})]\boldsymbol{I}, \tag{4}$$

where $\mu(\phi)$ is the suspension viscosity, and $p(\phi)$ accounts for the particle concentration dependence of the normal stress. The parameters w_t and w_g scale the relative magnitudes of the fluctuational velocity and shearing force contributions to $\boldsymbol{\Pi}$. To close the set of equations a conservation equation for the particulate-phase kinetic energy is written whose solution is the particle-phase temperature profile (McTigue & Jenkins 1992; Nott & Brady 1994).

For fully developed two-dimensional channel flow all three models predict non-uniform concentration and blunted velocity profiles, which are quantitatively similar to those measured experimentally. Owing to the symmetry of the flow and the lack of any accounting for the finite size of the suspended particles, the diffusive flux and Mills & Snabre models predict respective centreline concentrations equal to ϕ_m and ϕ^* regardless of the particle concentration in the bulk. Moreover, the diffusive flux model also predicts a sharp cusp in the profile for $\phi_{bulk} \leqslant 0.40$. Although this cusp can be eliminated by incorporating a larger value of χ than that measured within a wide-gap Couette flow (Phan-Thien *et al.* 1996), there is no justification for its use so far as we are aware.

On the other hand the spatial dependence of the particle normal stress in the Mills & Snabre and suspension balance models results in concentration profiles that do not possess a cusp along the conduit axis. By accounting explicitly for the size of the suspended particles, the suspension balance model actually predicts conduit centreline concentrations that are less than the divergent viscosity value. While it can be concluded that the Mills & Snabre and suspension balance models have successfully overcome the qualitative deficiencies of the diffusive flux model, Hampton *et al.* have reported better agreement of the diffusive flux model with their tube flow data.

In this paper we report experimental data for the concentration, particle velocity, and time-average squared fluctuational velocity (one component of the 'suspension temperature') distributions for a constant-volume-flux flow of concentrated Newtonian suspensions of neutrally buoyant monodisperse spherical particles through a parallel-wall channel that closely approximates two-dimensional pressure driven flow. We utilize a modified laser Doppler velocimetry technique that was developed within our lab (Lyon 1997), which enables flow field access up to particle volume fractions of 0.50. In addition to reporting the qualitative influence of the volumetric flow rate, the bulk particle concentration, and the ratio of channel gap width to particle diameter on the form of the fully developed profiles, we also compare calculated model predictions with our data in order to evaluate their quantitative usefulness for predicting suspension flow properties.

2. Experimental method

There are a large number of non-intrusive experimental methods which have been developed for measuring dynamic and/or microstructural properties of concentrated suspensions. These include Doppler velocimetry methods that utilize laser light (Chung 1980; Koh *et al.* 1994; Hookham 1985; Kapoor & Acrivos 1995; Jana *et al.* 1995; Averbakh *et al.* 1997), and acoustic radiation (Atkinson & Kytomaa 1993; Kowalewski 1980), as well as imagining techniques that incorporate nuclear magnetic resonance (Abbott *et al.* 1991; Corbett *et al.* 1995; Sinton & Chow 1991; Hampton *et al.* 1997;

Ding *et al*. 1993; Altobelli *et al*. 1991), visible light (Karnis *et al*. 1966; Leighton & Rampall 1993), and acoustic waves (Kytomaa & Corrington 1994; Matin *et al*. 1995; Bacri *et al*. 1991). The experimental method chosen for this study was a modified laser Doppler velocimetry (LDV) technique, which incorporates index-of-refraction matching of the suspending and particulate phases. One advantage of this method is its superior spatial resolution, which is an order of magnitude greater than what is typically found for the imaging and acoustic Doppler methods mentioned above. This higher resolution translates into a smaller suspension volume being needed to conduct experiments, which significantly reduces the effort required to obtain a sufficient number of particles having a narrow size distribution. A second benefit of LDV for channel or tube flows is the ease with which reliable concentration data can be obtained by measuring the inter-arrival time between consecutive particles traversing the probe volume. Finally, our LDV method measures the velocity of individual particles with such a high degree of spatial resolution that we are able to extract the time-average square velocity fluctuation of the particulate phase from the measured particle velocity data. These velocity fluctuations are one component of the temperature distribution utilized by the suspension balance model to account for the formation of a non-uniform particle concentration distribution. Experimental data verifying their existence, however, have, to our knowledge, not been previously reported.

To carry out this study, we have designed and built a one-dimensional LDV optical train that maximizes spatial resolution while still allowing access to all positions across the approximate 1 mm gap width of our channels. In order to overcome turbidity effects which hinder data acquisition we have developed an index-of-refraction-matched suspending fluid/particle system, which we briefly describe in the next subsection. In §2.2 we discuss the experimental apparatus used to obtain our particle velocity, concentration, and time-average square fluctuational velocity profiles. Finally, in §2.3 we provide a conservative estimate of our system's spatial resolution which justifies the reporting of profiles for the time-average square particle velocity fluctuations.

2.1. *Index-of-refraction match*

The object of the present study is to obtain experimental velocity data from suspensions of large particles (approximate diameters 50–100 μm) at high concentrations (volume fractions as high as 0.50), utilizing LDV. In order to overcome particle turbidity effects associated with the high concentrations of interest, we employ an optimal index-of-refraction match of the particulate and suspending phases. Since a perfect match is impossible due to microscale inhomogeneities within the particles' matrix, the term 'optimal' refers to the suspending-liquid index of refraction that maximizes light transmission through the suspension at the specified experimental conditions (temperature, incident wavelength, etc.). It is, in fact, these local regions of refractive-index mismatch that are presumably responsible for the scattered light signal. The principle benefit of this 'optimal' match is a minimization of secondary scattering by particles lying outside the probe volume, while still retaining sufficient scattered light from individual particles that traverse the probe volume.

In conjunction with index-of-refraction matching, we also employ density matching to eliminate flow effects associated with non-neutrally buoyant particles. A system we have developed to satisfy these requirements is similar to that reported by Graham *et al*. (1991), in which polymethyl methacrylate (PMMA) microspheres have been used as our particulate phase, and UCON oils and Triton X-100 are components of our suspending liquid. Particles of PMMA were chosen not only for their commercial availability, but also because PMMA possess a much lower index of refraction than

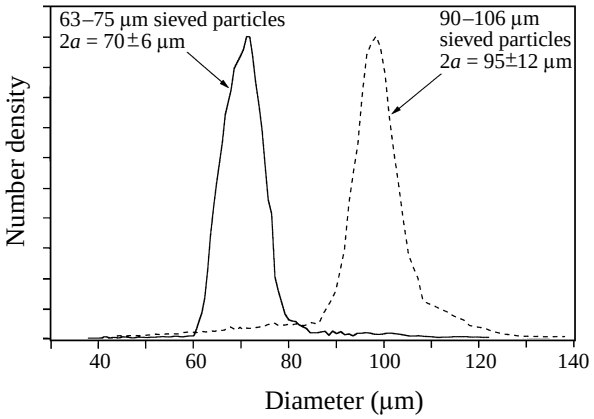

FIGURE 1. Nominal size distributions of the sieved poly(methyl methacrylate) microspheres.

polystyrene (the other widely available particle matrix), which allows the use of a greater number of potential liquid reagents for a density- and index-of-refraction matched suspension. UCON oils and Triton X-100 were chosen because they do not react chemically with PMMA, they possess low toxicity (classified as irritants), and they are known to respond as Newtonian fluids for the range of shear rates encountered within our flow channel. The final component of our suspending fluid, which was required to have a greater density and index of refraction than the PMMA microspheres, was 1,6-dibromohexane (Aldrich catalogue no. D4,100-7). This reagent possesses low toxicity (irritant), was miscible with the other liquid components, and reacts only slightly with PMMA (Lyon 1997).

The PMMA particles were purchased in one kilogram lots from Bangs Laboratories, and as delivered possessed a distribution of diameters in a range of 30–150 μm. Since suspensions of near monodisperse particles size were of interest in this work, two sets of particles with respective diameter ranges of 63–75 and 90–106 μm were separated using stainless steel sieves (Fisher Scientific) and an Octagon 2000 (CSC Scientific) electromagnetic sieve shaker. Typical size distributions for samples taken from these lots were measured with a Coulter counter, and are presented in figure 1. The number-average diameters for these distributions were found to be 70 ± 6 and 95 ± 12 μm, respectively.

In order to determine the suspending-fluid composition that provided an optimal index-of-refraction match with the particles, transmission experiments similar to those of Koh (1991) were performed on 1% suspensions of 90–106 μm diameter particles immersed in a series of suspending fluids whose density was equal to that of the particles (1.19 g cm^{-3}), and whose index of refraction ranged from 1.4865 to 1.4912 (at 20.0 ± 0.2 °C). The results of these experiments revealed a maximum transmission of approximately 0.95 (relative to the particle-free suspending liquid) for a suspending-fluid index of refraction between 1.4873 and 1.4878. Moreover, subsequent experiments conducted to test the stability of these suspension mixtures revealed that the liquid component index of the refraction was actually 0.0003 below what was mixed for the transmission experiments, where this decrease is believed to have resulted from the absorption of a small amount of 1,6-dibromohexane by the particles. Thus, the proper suspending-liquid index of refraction range for optimal matching was actually 1.4870–1.4875. Consequently, all the experiments were performed with a suspending-liquid index of refraction that was equal to 1.4873 ± 0.0001.

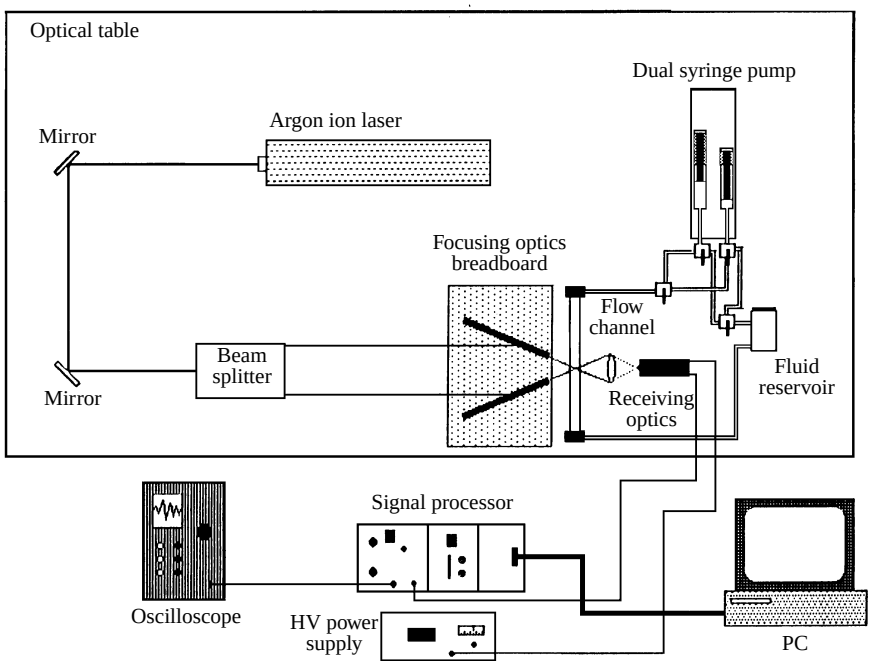

FIGURE 2. Schematic of LDA experimental apparatus.

Under the assumption of an ideal solution mixture, the corresponding suspending liquid composition for optimal matching of the particles' index of refraction and density is 50.0% Triton X-100, 23.0% 1,6-dibromohexane, and 27.0% UCON 75-H series lubricant. This latter component was 50:50 mixture of 75-H-450 and 75-H-90000 oils, which were used because of their availability within our lab, and because they produced a suspending liquid that was sufficiently viscous to render particle–liquid inertial effects negligible over the length of our channel, but not too viscous so that the suspensions could be pumped and degassed after being loaded into the flow system. When subjected to simple shear flow in the Couette device of a dynamic stress rheometer (Rheometric Scientific), this suspending fluid displayed a Newtonian response over five decades of shear, with a viscosity of 4.8 P at 20.0 °C. Finally, the measured temperature dependence of this suspending-fluid index of refraction and density required that the temperature within the lab not deviate by more than ± 1 °C.

2.2. *Experimental apparatus*

The entire set-up is illustrated in figure 2, and consists of optical, flow, and data processing systems. As is shown, the first two are attached to a pneumatically elevated optical table (Newport Research MST-48) in order to isolate the experimental measurements from external vibrations.

The light source of the optical system was an argon ion laser (Spectra Physics model 165), operated at a wavelength of 488 nm. Scattered light signals were collected by a 50 mm focal length camera lens (Nikon) operating at f1.4. The focused light was directed onto a bialkyl head-on photomultiplier tube (Hammatsu R1166), which was chosen for its combination of low dark current and high sensitivity to the scattered-light wavelength. Located between the lens and photomultiplier tube was a laser-line filter (Oriel) centred about 488 nm, as well as a 10 mm diameter pinhole. These last two

components were used to attenuate the effects of room light and keep stray laser light from striking the surface of the photomultiplier tube.

The focusing optics consisted of two 1 in. diameter mirrors (Melles Griot) that steered the beams emanating from the beam-splitter into two 1 in. diameter, 50 mm focal length lenses (Oriel). These four optical components rested on subminiature rails (Ealing Electro Optics) that were attached to the 1 ft $\times$ 2 ft $\times$ 2 in. optical breadboard (Melles Griot) shown in figure 2. The mirrors and lenses were attached to the breadboard surface utilizing subminiature mounts (Newport–Klingler), posts and post-holders (Melles Griot), and subminiature carriers (Ealing Electro Optics). Sandwiched in-between the carriers and post-holders were subminiature stages (Ealing Electro Optics), which combined with the aforementioned optical mounts resulted in four and five degrees of positioning freedom for each mirror and lens, respectively.

The flow channels were constructed from two 12 in. $\times$ 2 in. $\times$ 1/4 in. ground and polished optical glass plates (Rolyn Optics), and two machined 12 in. $\times$ 1/2 in. $\times$ 1/16 in. or 1/32 in. Plexiglas spacers. The glass plates possessed an anti-reflective coating, which was incorporated to reduce the level of noise resulting from the collection of reflected light during LDV measurements near the wall. The channels were held within the flow system by a machined anodized aluminium holder and capped by flow blocks, which were designed and built by Koh (1991). Two channels were constructed by cementing the lucite spacers to the glass plates with high-strength epoxy, which was necessary to prevent leakage resulting from dynamic pressure on the glass surfaces. The widths of the two channel gaps were measured with a microscope and found to be 1.0 and 1.70 mm, respectively.

The flow of suspension was generated by a dual syringe pump (Harvard Apparatus model 923) operating in a reciprocating mode. This pump was ordered with a modified gear box which enabled it to produce volumetric flow rates up to 114 $cm^3\ min^{-1}$ at a maximum pressure of 120 p.s.i. The pump also came equipped with two 50 cm^3 stainless steel syringes, since glass syringes were likely to burst at the high pressures required to pump the concentrated suspensions of interest. The reservoir was a modified 100 ml Pyrex glass bottle to which inlet and outlet glass flow ports were added. The reservoir serves a dual purpose: it ensures that a well-mixed suspension enters the flow channel, and also provides a medium through which entrained air bubbles can rise and escape to the atmosphere. All the connecting tubing was flexible, inert 1/4 in. OD Teflon tubing that had 1/40 in. thick walls. Connections to the inlet and outlet of the reservoir were accomplished by clamping this tubing inside short sections of 3/8 in. OD, 1/16 in. wall thickness Teflon tubing, which was pressed onto the ports and clamped to prevent leakage. The remaining flow system components were connected to the Teflon tubing with stainless steel and brass swage-lock fittings.

With the exception of experiment 008, all the data were processed by a counter signal processor (TSI model 1980B). Provided the signal strength from the photomultiplier tube exceeded the 50 mV threshold voltage level required to trigger the processor to continue making a frequency measurement, the processor bandpass filtered the signal over the range 1–100 kHz in order to remove the low-frequency pedestal component, as well any high-frequency noise introduced into the signal by the photomultiplier tube or processor amplifier electronics. The remaining signal was then digitized for measurement of the Doppler frequency. A valid signal was required to possess five or more cycles, which were counted along with the total time ($+2$ ns precision) required for those cycles. Simultaneously, the time between the previous and present particle bursts was also measured. The resulting data (the number of cycles N, the signal duration time t_s, and the time between consecutive Doppler bursts t_{bd}) was sent directly

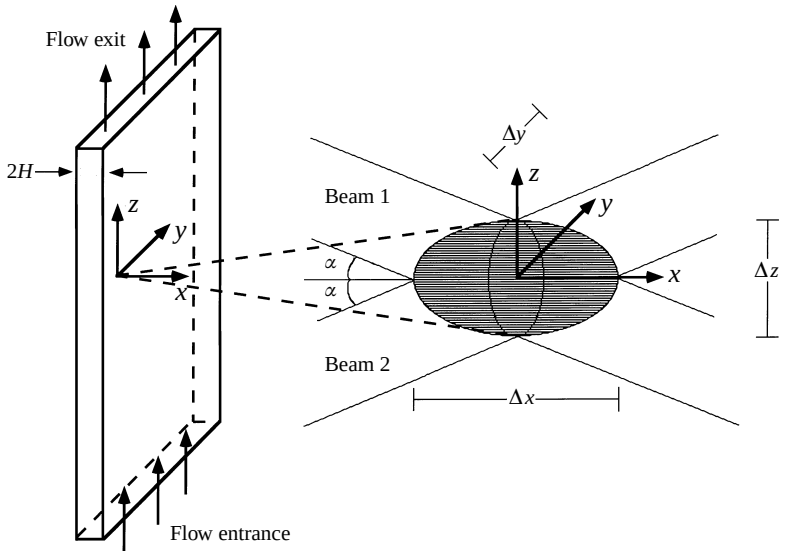

FIGURE 3. Schematic of the LDA ellipsoidal probe volume and the flow system coordinate system.

to computer storage (PC-AT), which controlled data acquisition and performed initial data reduction through FORTRAN programs written by Koh (1991).

Data for experiment 008 were processed using a digital signal processor (TSI model IFA 655). This processor received the voltage signals from the photomultiplier tube, and sent them through a bandpass filter over a range of 1–30 kHz. Next, the signal was amplified, digitized and validated via signal-to-noise ratio monitoring and an input threshold voltage setting of 50 mV. The processor determined the Doppler frequency by a double-clipped autocorrelation technique (TSI 1995), and recorded the time between consecutive bursts. Like the counter processor set-up, the number of cycles N, signal duration time t_s, and time between consecutive bursts t_{bd}, were sent directly to computer storage (75 MHz Pentium, Gateway 2000). The computer controlled processor settings, data acquisition, and performed data reduction through FORTRAN programs and Excel spreadsheets. By setting the required detection signal-to-noise ratio level to 'high', this processor acquired data in a manner that was nearly identical to the counter processor used for the other experiments.

2.3 *Probe volume estimate*

Since our signal processors required that the amplitude of a burst exceed a threshold value in order to record a frequency measurement, the size of the measuring volume depends upon the focusing and power of the illuminating laser beams, the particle scattering properties, the light collection efficiency of the receiving lens, and the sensitivity and amplification of the processing electronics (Adrian 1980). For these experiments all of the above were known or could be estimated, except for the particle scattering properties, which were ambiguous since Mie scattering theory requires non-zero values of the relative refractive index and knowledge of the area responsible for scattering the laser light.

Instead, the dimensions of the probe volume seen by the detector will be reported for the case in which the beam crossing occurs within the suspension medium. This region is the intersection of the cone formed by the image of the pinhole through the collection lens and the elipsoidal region of the two crossed and focused Gaussian beams, whose

irradience is e^{-2} of its maximum value (i.e. the irradience at the intersection of the two beams along their axes). Since this optical arrangement is not self-aligning like a single focusing lens system, the size of the ellipsoid region is estimated by assuming that the two beams cross within the Rayleigh length of each focused beam. That is, we assume the diameter of each beam at the crossover region is within $\sqrt{2}$ of its diffraction-limited value.

An estimate of the probe volume is then based upon this approximation in addition to the following: first, the beam crossing half-angle was limited to 0.28 radians by the physical size of the optical mounts holding the focusing lenses; second the utilized collection lens magnification of 1.4; and third the assumption that the receiving optics lie within the $(x\,y)$-plane at a 5° angle defined with respect to the x-axis of figure 3. The result for the probe volume whose major axes within view of the detector is

$$\Delta x = 42\ \mu\text{m}, \quad \Delta y = 7.2\ \mu\text{m}, \quad \Delta z = 7.2\ \mu\text{m}. \tag{5}$$

This result verifies the assertion that our system is capable of measuring particle velocity and concentrations on length scales smaller than the size of our suspended particles.

3. Experimental procedure

3.1. *Suspension preparation*

Suspensions were prepared by adding the appropriate masses of particles and suspending fluid in a 250 ml glass Pyrex bottle (Fisher). A total suspension mass of approximately 300 g was required to fill the flow system. To ensure that the LDV data resulted from scattering due to the presence of the suspended PMMA particles, the suspending liquid was high pressure filtered through a 0.22 μm pore size filter (Millipore) prior to being mixed with the particles. The suspension was then mixed for about three hours, at which time the particles were dispersed within the suspending liquid. In order to overcome absorption of the 1,6-dibromohexane by the suspended particles, a few millilitres of 1,6-dibromohexane/Triton X-100 solution, which had the same density as the PMMA particles but a higher index of refraction, was added until the aforementioned 'optimal' suspending liquid index of refraction was achieved. Additional particles were then mixed into the suspension in order to obtain the desired bulk particle concentration for the experiment of interest.

3.2. *Data acquisition*

Data acquisition was initiated by positioning the flow channel such that the probe volume was within approximately 75 μm of one of the walls. Subsequent channel gap positions were then accessed by translating the channel in discrete 75 μm increments until the opposite wall was reached. Typically, 100 data points were collected near the wall, while in the region of the channel axis 1000 velocity and inter-arrival times were recorded. Because statistically indistinguishable profiles were found for experiments in which nearly five times as many data points were collected at each position within the gap, a sufficient number of bursts were sampled for proper characterization of the velocity, concentration and time-average square velocity fluctuation profiles.

4. Testing the experimental system

Prior to each suspension experiment, the alignment of the optical system was tested by measuring the velocity profile of a Newtonian liquid across the channel gap. This was accomplished by seeding the flow system with 6 mm diameter polystyrene particles

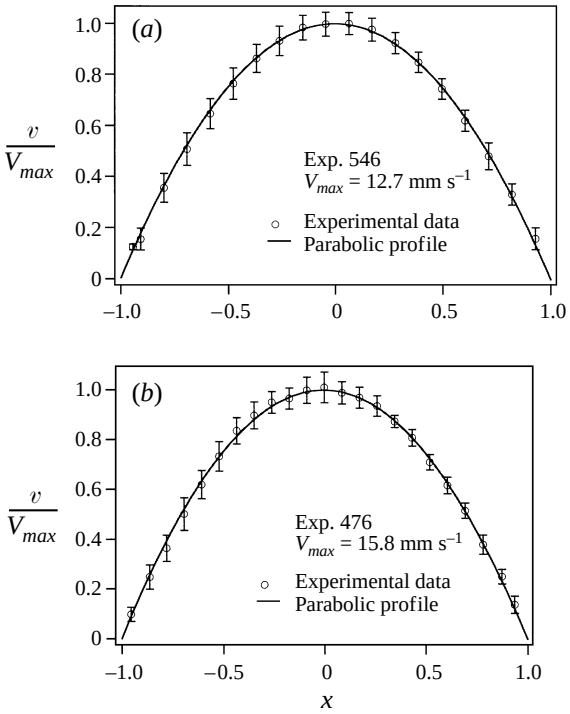

FIGURE 4. Measured velocity profiles for water seeded with 6 μm diameter polystyrene microspheres: (*a*) $2H = 1.0$ mm, $\langle\dot{\gamma}\rangle = 51.7$ s^{-1}; (*b*) $2H = 1.7$ mm, $\langle\dot{\gamma}\rangle = 37.2$ s^{-1}.

(Polysciences), and measuring approximately 200 data points at roughly 20 spatial positions across the channel gap. Because channel aspect ratios of 0.02 and 0.032 were utilized, the flow across the channel gap was approximately two-dimensional, and therefore, a parabolic velocity profile was expected.

Two typical sets of Newtonian data, one for each of the channels used, are presented in figure 4. The velocity values of the ordinate within each plot were normalized by the maximum velocity at the channel centreline, V_{max}, and the spatial position on the abscissa by the gap half-width, H. The solid line in the plots is the theoretical parabolic profile, while the error bars represent one standard deviation in the collected data. The complete agreement between the experimental and theoretical profiles clearly reflects the high spatial resolution of the system, particularly since the average shear rate across the gap for these two experiments is one order of magnitude above the generally accepted maximum value of 1 s^{-1} that is ascribed to LDV.

5. Data reduction

5.1. *Velocity measurement*

Intrinsic to LDA is an absolute measure of the local velocity of a particle as it crosses the probe volume formed by the two crossed laser beams. For the one-dimensional system incorporated here, the velocity of individual particles in the direction of flow (i.e. the z-component of figure 3) v_{p_i}, was measured. Of interest was the average velocity $\overline{v_p}(x)$, and standard deviation of these measurements at each spatial position within the channel gap. These values were calculated from the total number of particles measured at each respective position, and then normalized by the centreline velocity for a Newtonian fluid (water) and an identical flow rate.

5.2. *Local concentration measurement*

Measurement of the local particle concentration results from the existence of a Poisson distribution of particles within the flow that scatter sufficient light to overcome the voltage threshold of the signal processor. The existence of this random distribution was deduced from the observation of a zero correlation time for the measured inter-arrival times of particles through the probe volume. Utilizing Poisson statistics, it can be shown that the average distance between consecutive measurable particles in the direction of flow is inversely proportional to the average concentration of particles at the gap position of interest (Lyon 1997).

Experimentally, the average distance between scattering particles is calculated by averaging the product of the time between consecutive particles passing through the probe volume and the velocity of the latter particle,

$$\bar{r}(x) = \frac{1}{N-1}\sum_{i=2}^{N} v_{p_i} t_{bd_1} = \overline{v_p(x)\, t_{bd}(x)}. \tag{6}$$

Noting that the average local particle volume fraction at x, $\bar{\phi}(x)$, is inversely proportional to the local average distance between particles yields

$$\bar{\phi}(x) = \frac{k}{\overline{v_p(x)\, t_{bd}(x)}}, \tag{7}$$

where k is a constant of proportionality. The value of k is found from the known volume flux of particles through the channel,

$$k = \frac{\phi_{bulk}\, Q}{\displaystyle\int_{-1}^{1} \overline{t_{bd}}(x)\, \mathrm{d}x}, \tag{8}$$

where Q is the dimensionless volumetric flow rate supplied by the pump, and is equal to $4/3$ for the two-dimensional channel flow considered. The limits of integration in (8) represent the dimensionless wall positions of the channel gap over which the measurements are made.

It is important to discuss the implications of writing (8) relative to previous suspension flow studies within our lab (Hookham 1986; Koh *et al.* 1994). In normalizing their concentration data these investigators assumed that the average volume fraction at each cross-section of their conduit was equal to ϕ_{bulk}. This normalization condition is incorrect, however, because on average a particle has a shorter residence time within the channel than an equivalent volume of fluid due to the net migration of particles from slower moving streamlines near the wall toward faster moving ones near the channel axis. Moreover, measurements of the difference between the particle concentration in the bulk and inside the tube (Chapman 1990; Seshadri & Sutera 1968) reveal that the error associated with using this average concentration constraint can be as high as 15% for the ratio of particle size to conduit dimension (tube diameter or channel gap width) and bulk particle concentration encountered in this study.

5.3. *Time-average squared velocity fluctuations*

Since LDV measures velocity data from individual particles as they traverse the probe volume, it is possible to extract the time-averaged squared velocity fluctuation resulting

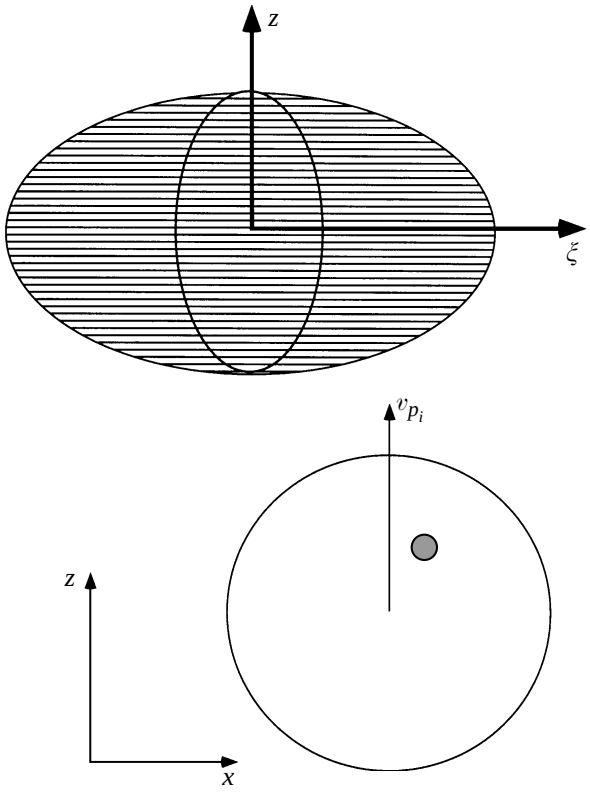

FIGURE 5. Schematic of a particle crossing the edge of the probe volume for estimating the fluctuational velocity resulting from the finite size of the probe volume.

from hydrodynamic interactions between particles from the overall mean-square fluctuation, which is defined at a position within the channel gap as

$$\overline{(v'^2)}(x) \equiv \frac{1}{N}\sum_{i=1}^{N} v'^2_{p_i}(x) = \frac{1}{N}\sum_{i=1}^{N} (v_{p_i}(x) - \overline{v_p}(x))^2 = \overline{v_p^2}(x) - \overline{v_p}^2(x). \tag{9}$$

In writing (9) the time average is represented experimentally by an average over N particle measurements.

The source of velocity fluctuation in the LDA data is not entirely due to interactions between the suspended particles. Inherent to the experimental method are velocity variations resulting from a finite-sized probe volume over which a non-zero velocity gradient exists, the rotational velocity of the particles, and volumetric flow rate fluctuations resulting from irregularities on the lead screw of the syringe pump. The second source of velocity fluctuation occurs because the source of scattered light is not necessarily coincident with the centre of mass (or rotation) of the particle for these refractive-index-matched systems, i.e. scattering presumably occurs from local variations of the refractive index within the particles. On average, the particles possess an angular velocity that is roughly half the local shear rate measured at their centre of mass (Goldsmith & Mason 1967). Assuming that the average distance between the scattering point and the centre of mass of a typical measurable particles is $a/2$, the time-average squared velocity fluctuation resulting from particle rotation should scale as $O(\dot{\gamma}^2 a^2/16)$. This is one order of magnitude lower than the anticipated result for

particle interactions (Nott & Brady 1994). Based upon this argument, we shall assume that the time-average squared fluctuation in particle velocity resulting from the angular motion of the particles is negligible.

Evidence for the existence of velocity fluctuations resulting from the pump was obtained by computing the power spectrum of velocity data at one position within the channel gap. Resulting from these calculations was a predominant frequency that corresponded to the lead screw's angular velocity. It will be argued below, however, that the magnitude of these pump fluctuations is also negligible relative to those resulting from particle interactions. Assuming this to be true, the analysis below only considers contributions due to particle interactions and variations resulting from the presence of a velocity gradient across a finite-sized scattering volume. We denote these two contributions for particle i, as $v_{p_i}^{int}$ and $v_{p_i}^{pv}$, respectively, and assume the overall velocity fluctuation can be expressed as a sum of these two terms,

$$v'_{p_i}(x) = v_{p_i}^{int}(x) + v_{p_i}^{pv}(x). \tag{10}$$

The fluctuational terms on the right-hand side of (10) are written with a spatial dependence transverse to the flow direction, because there exists a non-uniform concentration distribution and a spatially varying velocity gradient across the channel gap. Substituting the above into (9), expanding the summation, and solving for $\overline{(v_p^{int})^2}$ produces an expression for the time-averaged squared velocity fluctuation of the particles resulting from hydrodynamic interactions,

$$\overline{(v_p^{int})^2}(x) = \overline{v_p^2}(x) - \overline{v_p}^2 - \overline{(v_p^{pv})^2}(x) \tag{11}$$

Note that (11) does not contain any time-averaged fluctuational terms resulting from products of the two fluctuational sources, because the different fluctuational sources are assumed to be uncorrelated.

To estimate $\overline{(v_p^{pv})^2}$ consider the situation shown in figure 5, in which a suspended particle with a local index-of-refraction mismatch traverses the probe volume with a trajectory that brings the mismatch region of the particle to within a distance ξ from the centre of the probe volume. We assume that the velocity gradient $\dot{\gamma}(\xi)$ that exists across the probe volume is uniform, which is justified by the fact that the linear dimensions of the scattering volume are small compared to the width of the channel gap. The particle velocity at ξ is then calculated relative to that at the centre of the probe volume via

$$v_{p_i}(\xi) = v_p(\xi = 0) + \xi\dot{\gamma}, \tag{12}$$

where $v_p(\xi = 0)$ is the particle velocity when the particle's index-of-refraction mismatch crosses the centre of the probe volume.

The last term on the right-hand side of (12) is simply an approximation for the velocity fluctuation of particle i resulting from the existence of the velocity gradient over the probe volume. The time-averaged fluctuational velocity resulting from the finite size of the probe volume is then determined by summing over the N sampled particles,

$$\overline{(v_p^{pv})^2} = \frac{1}{N}\sum_{i=1}^{N}(v_{p_i}^{pv})^2 = \sum_{i=1}^{N}\xi_i^2\,\dot{\gamma}^2. \tag{13}$$

However, the N values of ξ_i are unknown from the experimental data. Therefore, we will transform the summation over all measured particles into an integral over the

length of the probe volume using the spatially varying particle flux through the probe volume as a weighting function, That is,

$$\overline{(v_p^{pv})^2} = \frac{\int_{-\delta}^{\delta} v_p(\xi)\,\phi(\xi)\,(v_{p_i}^{pv})^2(\xi)\,\mathrm{d}\xi}{\int_{-\delta}^{\delta} v_p(\xi)\,\phi(\xi)\,\mathrm{d}\xi}, \tag{14}$$

where 2δ is the length of the probe volume in the cross-stream direction. Using Taylor series approximations for the local particle velocity and concentration fields within the integrals of (14), and keeping terms to the lowest order of δ after integration yields

$$\overline{(v_p^{pv})^2} \approx \frac{\delta^2\dot{\gamma}^2}{3} - O[\delta^4]. \tag{15}$$

Substituting (15) into (11) then yields an approximation for the time-average squared fluctuational velocity associated with particle interactions,

$$\overline{(v_p^{int})^2}(x) \approx \overline{v_p^2}(x) - \overline{v_p}^2(x) - \tfrac{1}{3}\delta^2\dot{\gamma}(x)^2. \tag{16}$$

To make this expression dimensionless, we use H and V_{max} as our respective characteristic length and velocity scales. Since $(v_p^{int})^2$ is expected to scale as $(a/H)^2\,V_{max}^2$ (Nott & Brady 1994), we use this to scale the left-hand side of (16). The resulting dimensionless equation for extracting the time-average squared fluctuational velocity associated with particle–particle interactions then becomes

$$\overline{(v_p^{int})^2}(x) \approx \left(\frac{H}{a}\right)^2 (\overline{v_p^2}(x) - \overline{v_p}^2(x)) - \frac{1}{3}\left(\frac{\delta}{a}\right)^2 \dot{\gamma}(x)^2 - O\left[\left(\frac{\delta}{a}\right)^4\right]. \tag{17}$$

Finally, a few comments concerning velocity fluctuations resulting from the pump are warranted. Since a constant-displacement pump was used, any fluctuations originating from its operation appear as fluctuations in the volumetric flow rate, Q_s. Moreover, since the suspension velocity at any point within the channel gap is proportional to Q_s and decreases monotonically across the gap from the channel axis to the walls, so too should any fluctuations in velocity which occur as a result of fluctuations in the volumetric flow rate. Therefore, the maximum and minimum pump contribution to the time-average squared velocity fluctuation should occur at the channel axis and walls respectively. Since the velocity gradient at the channel axis is zero owing to symmetry, the maximum value for the pump mean square fluctuational velocity is from (17),

$$(\overline{v_p^{pump})^2})_{\max} = \left(\frac{H}{a}\right)^2 (\overline{v_p^2}(0) - \overline{v_p}^2(0)). \tag{18}$$

As will be shown in §6.1 (see figure 6), a typical experimental profile resulting from (17) possesses a minimum value of $\overline{(v_p^{int})^2}(x)$ at the channel axis. Therefore, the result given by (18) provides an upper limit on the mean square fluctuational velocity resulting from the pump. Moreover, this near axis value is small, and consequently, pump fluctuations have little effect on the qualitative shape of the $\overline{(\mathrm{v_p^{int}})^2}(\mathrm{x})$ profile.

6. Results and discussion

The goal of this work is measurement of the coupled steady-state velocity, concentration, and time-average squared fluctuational velocity profiles across the

Experiment number	ϕ_{bulk}	Q_s (ml min^{-1})	Re_p ($\times 10^{-6}$)	H/a	$[L/H]_{ss}$	$[L/H]_{exp}$
563	0.30	8.2	12.0	11	38	380
539	0.30	8.2	4.9	14	71	380
562	0.30	12.2	3.6	18	111	224
463	0.30	12.2	1.5	24	200	280
464	0.30	23.6	2.9	24	200	280
478	0.35	23.6	2.9	24	99	280
479	0.35	12.2	1.5	24	99	280
572	0.40	8.2	12.0	11	10	380
538	0.40	8.2	4.9	14	18	380
553	0.40	12.2	3.6	18	28	224
482	0.40	12.2	1.5	24	50	280
483	0.40	23.6	2.9	24	50	280
484	0.45	12.2	1.5	24	26	280
486	0.45	23.6	2.9	24	26	280
550	0.50	8.2	12.0	11	3	380
575	0.50	8.2	4.9	14	5	380
551	0.50	12.2	3.6	18	8	224
008	0.50	12.2	1.4	24	14	220

TABLE 1. Experimental parameters. The last two columns are the scaling-based relative downstream channel positions required for the measurement of fully developed profiles, and the experimental values that were incorporated, respectively.

narrow gap of the flow channels. For the large particles employed in this study, Brownian and colloidal forces are negligible, while buoyancy forces are non-existent owing to density matching of the two phases. Particle concentration non-uniformities resulting from inertial interactions between the fluid and particles were also rendered negligible over the length of the channel by our choice of experimental parameters. That is, the particle Reynolds number defined in a manner analogous to that for tube flow (Goldsmith & Mason 1967),

$$Re_p \equiv \frac{4}{3}\frac{\rho}{\mu}\frac{a^3}{H^2}V_{max}, \tag{19}$$

is no larger than 10^{-5}.

Of particular interest was the dependence of the measured steady-state profiles on the volumetric flow rate Q_s, the volume (or mass) fraction of particles in the bulk suspension ϕ_{bulk}, and the ratio of channel gap width to particle diameter, 2H/2a. To complete these objectives, the eighteen experiments listed in table 1 were conducted, which encompassed two distinct flow rates, bulk particle concentrations ranging from 0.3 to 0.5, and channel gap widths equal to 11, 14, 18, and 24 particle diameters. In order to probe the effect of flow rate on the steady-state profiles, measurements were performed at 12.2 and 23.6 ml min^{-1} for $H/a = 24$ and ϕ_{bulk} values of 0.30, 0.35, 0.40, and 0.45. These data along with an additional experiment at $\phi_{bulk} = 0.50$ *and* $Q_s = 12.2$ ml min^{-1}, provided a set of data for the influence of bulk particle concentration on the fully developed profiles. Finally, in order to probe the influence of the relative channel gap width (or particle size), nine more experiments were performed at particle concentrations of 0.30, 0.40, and 0.50, and the last three H/a values.

A typical set of experimental data is presented in figure 6(*a–c*) where the local particle velocity, the concentration (i.e. volume fraction of particles), and the time-average squared velocity fluctuation due to particle interactions are plotted versus the

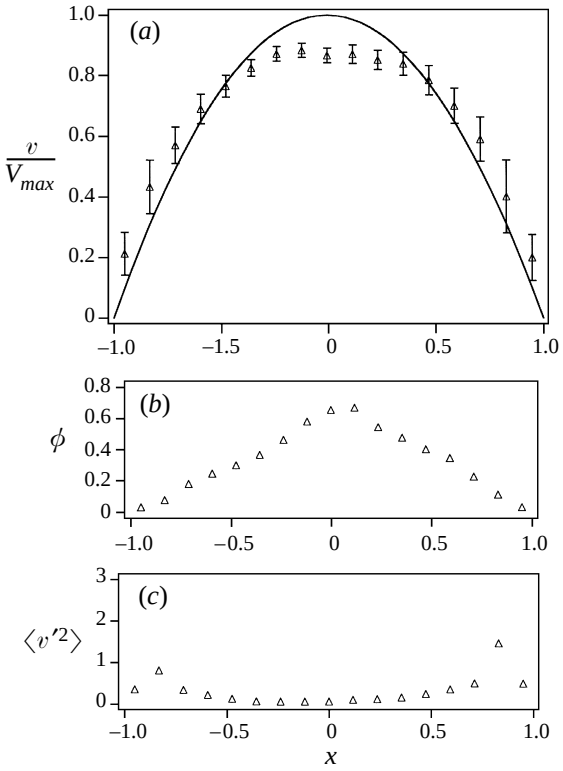

FIGURE 6. Particle velocity, concentration, and time-average squared velocity fluctuation profiles of experiment 572. Experimental parameters are: $Re_p = 1.2 \times 10^{-5}$, $\phi_{bulk} = 0.40$, $H/a = 11$.

dimensionless spatial position across the channel gap. The measured concentration distribution appears symmetric and non-uniform, with a maximum value near the channel axis and minima at each wall. The relative error in the concentration measurements is less than $\pm 10\,\%$, based upon the measured deviation in multiple concentration measurements at the same channel gap position. The symmetry of the concentration profile reflects the quality of the refractive index match. Otherwise, the probability of a particle being measured would not be constant across the gap, and nearly identical concentration values at positions equally spaced from the channel axis would not have been measured.

During the course of making concentration profile measurements on bidisperse systems (Lyon & Leal 1998), it was discovered that the LDV concentration values in the outer 20 % of the channel are lower than data obtained using optical microscopy. Moreover, the difference in the measured particle concentration in this region resulting from these two methods was found to increase at higher values of H/a, and more strongly with increasing ϕ_{bulk}. We believe that these lower particle concentrations are, at least partially, a consequence of an intrinsic property of LDV, namely, a lower signal-to-noise ratio near the walls (Adrian 1980). This decreases the probability of a particle being measured as it traverses the probe volume compared to the situation in which the same actual particle flux exists at a position near the channel axis. Therefore, the number of particles that were measured per unit time within this region was lower than the true value, and a lower relative concentration was measured. As a result of this inaccuracy, we can only report with confidence the concentration of particles within

the inner 80% of the channel gap. Using the normalization procedure of §5.2, the average impact of this inaccuracy on the reduced concentration data at spatial positions within $-0.8 \leqslant x \leqslant 0.8$ was found to be less than 2% for $0.30 \leqslant \phi_{bulk} \leqslant 0.40$ and less than 8% at $\phi_{bulk} = 0.50$.

The measured velocity profile represented by the symbols ($\triangle$) in figure 6(*a*) is blunted compared to the parabolic Newtonian result shown by the solid line. The error bars on the particle velocity data are one standard deviation in the data collected at each spatial position, which are composed of velocity fluctuations due to the finite size of the probe volume as well as particle interactions. The calculated time-average squared velocity fluctuation distribution resulting primarily from these latter fluctuations (shown in figure 6*c*), appear symmetric with a minimum near the channel axis, and peaks at approximately $x = \pm 0.8$ (these results are weakly dependent on the concentration profile error above). As will be seen in §6.3, this result is in qualitative agreement with the three-dimensional suspension temperature profile predicted by the suspension balance model.

6.1. *Conditions for the existence of fully developed profiles*

Prior to discussing the results for the range of parameters mentioned above, a necessary first step is to verify that our measured profiles are fully developed. For Poiseuille flows of concentrated suspensions ($\phi_{bulk} \geqslant 0.30$) there exists a total strain at which the resulting coupled concentration and velocity profiles reach fully developed forms. For channel flow this strain leads to an estimate for the dimensionless induction length $[L/H]_{ss}$ that the suspension should travel for fully developed profiles to be measured. Using scaling arguments Nott & Brady (1994) have shown that this length can be estimated by

$$\left[\frac{L}{H}\right]_{ss} \sim \frac{1}{12f(\phi)}\left(\frac{H}{a}\right)^2, \tag{20}$$

where it is assumed that a particle's average displacement between an initial uniform concentration distribution and the final fully developed state is one-quarter the channel gap width. The function $f(\phi)$ accounts for the bulk particle concentration dependence of the shear-induced coefficient of diffusion. Leighton & Acrivos (1987) and more recently Chapman (1990) have found that

$$f(\phi) = \tfrac{1}{3}\phi^2(1 + \tfrac{1}{2}\mathrm{e}^{8.8\phi}) \tag{21}$$

provided a good fit to their experimentally measured diffusion coefficients.

Equations (20) and (21) were utilized to determine the downstream position at which our velocity and concentration measurements are expected to yield fully developed profiles. Calculated values for $[L/H]_{\mathrm{ss}}$ as well as the corresponding experimental values $[L/H]_{exp}$ at each probed value of ϕ_{bulk} and H/a are also presented in table 1. With the exception of experiments at $\phi_{bulk} = 0.30$ and 0.35 and $H/a = 18$ and 24, these results show that the measuring position used for the experiments was at least five times farther downstream than the value computed from (20), which strongly suggests that the measured concentration distributions were fully developed.

In the case of experiments 463, 464, 478, 479, and 562, recent simulation results for the case of circular-tube flow (Hampton *et al.* 1997) suggest that these measurements should have occurred at a downstream position that was roughly twice that actually used. Because modification of the velocity profile for these experiments is relatively small (Phan-Thien & Fang 1996), the measured profiles are believed to be fully developed, while the concentration profiles are at worst 90% fully developed.

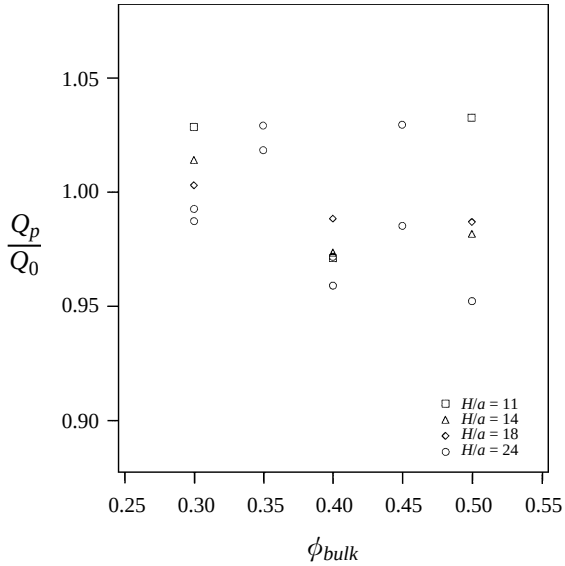

FIGURE 7. Particle flux results for the eighteen experiments of interest. The results suggest that the particles translate through the channel at the suspension phase-averaged velocity.

Moreover, as will be shown in §6.6, the concentration data of experiment 562 are in close agreement with the results of fully developed Stokesian Dynamics simulations at similar values of ϕ_{bulk} and H/a. Furthermore, the results obtained for experiments 463 and 464 are within experimental uncertainty of the data at lower H/a values, where this H/a independence of the measured concentration profile at $\phi_{bulk} = 0.30$ is consistent with analogous results at ϕ_{bulk} values of 0.40, and 0.50.

6.2. *Relative velocity of the particulate and suspending phases*

One significant issue in this work was whether the velocity of the particle phase lags behind that of the suspending liquid as has been reported for similar experiments performed within our lab (Koh *et al*. 1994). The presence of such a relative slip velocity is not consistent with the experimental results of Karnis *et al*. (1966), nor in agreement with the suspension balance model predictions of Nott & Brady (1994). To determine whether there is a significant slip indicated by the present data, the area under the particle velocity profile for each experiment has been calculated and normalized by the area under a parabolic Newtonian profile for identical flow conditions,

$$Q_r = \frac{3}{4}\int_{-1}^{1} v_p(x)\,\mathrm{d}x. \tag{22}$$

Results for all eighteen experiments, which are presented in figure 7, reveal that the dimensionless ratio Q_r for each experiment is within $\pm 5\%$ of unity, and independent of ϕ_{bulk} and H/a. This suggests that the particles do not lag behind the suspending fluid, but translate through the channel with a time-averaged local velocity that is equal to the time-averaged suspension velocity. In order to eliminate the small differences which do exist when comparing the results from different experiments or with model predictions, each set of velocity data will be rescaled so that the area under each velocity profile is equal to the area under a Newtonian parabolic profile, i.e. Q_r is unity.

Since the results reported in figure 7 differ from those of Koh *et al*. an explanation

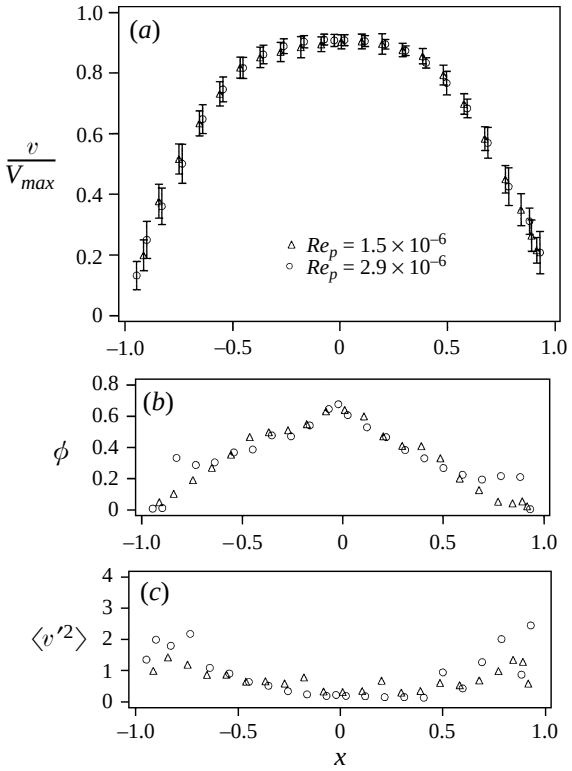

FIGURE 8. Influence of volumetric flow rate on the steady velocity, concentration, and time-average squared velocity fluctuation profiles for experiments 482 and 483, $\phi_{bulk} = 0.40$, $H/a = 24$.

for their observations is warranted. We believe their apparent slip velocity resulted from systematic errors in their experimental procedure. One such error may have been widening of their channel gap due to the high pressure required to pump their suspensions, and their inability to affix their lucite spacers to the glass plates that composed the channel walls. Since narrow gaps were employed, a widening of only a few hundred microns would have resulted in significantly lowered velocity measurements. Moreover, since the suspensions required pumping pressures that were at least two orders of magnitude larger than what was required to flow their base Newtonian liquid (water), this widening effect may have only occurred when the flow system was filled with suspension. A second potential source of error was their inability to sufficiently degas their flow system owing to the short period of time for which their index-of-refraction-matched suspensions were usable. The resulting deformation of entrained air within the flow system during each pump cycle would have produced a suspension flow rate that was below that prescribed by their pump. It is believed that these two sources of error were particularly responsible for their reported velocity data being in some cases as small as half the value reported elsewhere under similar experimental conditions (Hampton *et al.* 1997; Hookham 1986; Karnis *et al.* 1966).

6.3. *Influence of volumetric flow rate*

The influence of volumetric flow rate on the measured fully developed profiles is presented in figure 8 for a bulk particle concentration 0.40. It can be seen that the measured profiles are well within experimental uncertainty for the two values of Q_s that

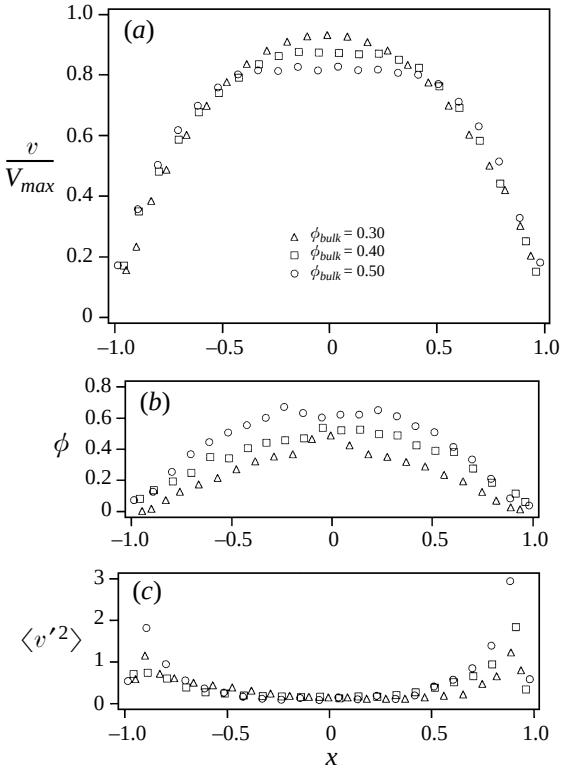

FIGURE 9. Influence of ϕ_{bulk} on the steady velocity, concentration, and time-average squared velocity fluctuation profiles for experiments 562, 553, and 551, $H/a = 18$ and $Re_p = 3.6 \times 10^{-6}$.

were investigated. This lack of flow-rate dependence on the steady profiles has also reported in other investigations (Koh *et al.* 1994; Karnis *et al.* 1966; Hampton *et al.* 1997), and is predicted theoretically by most models found in the literature (Buyevich 1996; Leighton 1985; Phillips *et al.* 1992; Mills & Snabre 1995; Nott & Brady 1994).

6.4. *Influence of bulk particle concentration*

The effect of ϕ_{bulk} on the measured fully developed profiles is illustrated n figure 9, where data at bulk particle volume fractions of 0.30, 0.40, and 0.50, and a channel gap width of 18 particle diameters are presented. As can be seen in figure 9(*b*), an increase in ϕ_{bulk} resulted in an increase in the concentration of particles within the central region of the channel, and a more pronounced blunting of the velocity profile. These observations are consistent with model predictions, in which greater velocity profile blunting is predicted at higher bulk particle concentrations due to the increasing sensitivity of the suspension viscosity on the local particle concentration.

The effect of ϕ_{bulk} on the time-average squared particle velocity fluctuation profile is illustrated in figure 9(*c*). The main effect is an increase of the near-wall maximum with increasing particle concentration. This behaviour is predicted by the suspension balance model, since the local fluctuational velocity scales with the local shear rate for a fixed value of H/a, and $\dot{\gamma}$ increases within the near-wall region with increasing ϕ_{bulk}. However, this result cannot be stated with confidence, because differentiation of the measured velocity profiles to calculate the local shear rate in (17) introduces significant uncertainty into the extracted time-average squared particle velocity fluctuation values.

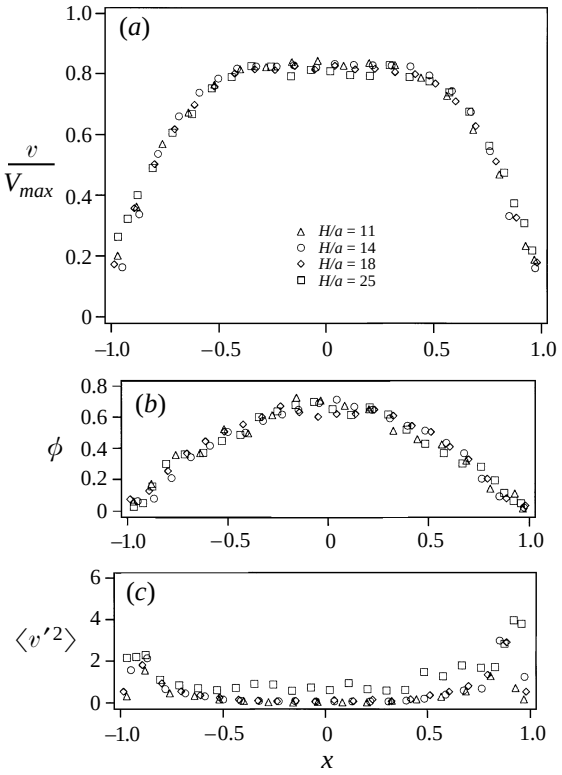

FIGURE 10. Influence of H/a on the steady velocity, concentration, and time-average squared velocity fluctuation profiles for experiments 008, 550, 551 and 575, $\phi_{bulk} = 0.50$, and $1.4 \times 10^{-6} \leqslant Re_p \leqslant 1.2 \times 10^{-5}$.

6.5. *Influence of the ratio of channel gap width to particle size*

Results for the four investigated values of H/a are presented for $\phi_{bulk} = 0.50$ in figure 10. For each value of ϕ_{bulk} probed the observed velocity and concentration profiles are within experimental uncertainty for the range of the relative channel gap width investigated. This apparent lack of H/a dependence is consistent with the diffusive flux and Mills & Snabre models, in which the fully developed profile equations for both models are independent of the particle size. On the other hand, the suspension balance model explicitly accounts for the physical size of the particles through the conservation of fluctuational energy. Because this predicted H/a dependence is weak, the narrow range of relative channel gap width investigated suggests differences that are within the uncertainty of the experimental technique. Finally, the uncertainty introduced in differentiating the velocity profile data that was noted above for the influence of ϕ_{bulk} on the time-average squared particle velocity fluctuation profiles suggests that results for the investigated range of H/a are also within experimental uncertainty. Therefore, we believe that the apparent trend of an increasing fluctuational energy near the axis of the channel with increasing H/a shown in figure 10(*c*), which coincidentally is opposite to the trend predicted by the suspension balance model, cannot be presented with any level of confidence.

6.6. *Comparisons with other data*

We now compare our results with previously reported data found in the research literature. More specifically, we compare our data with the Stokesian Dynamics

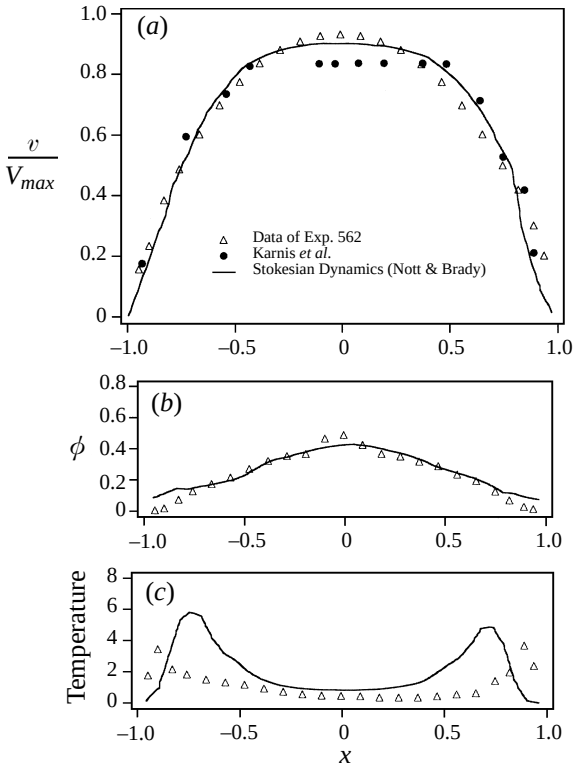

FIGURE 11. Comparison of results for $\phi_{bulk} = 0.30$, and $H/a = 18$ with Stokesian Dynamics simulation results of Nott & Brady for $\phi^a_{bulk} = 0.45$ and $H/a = 18.3$, as well as cinematography velocity data of Karnis *et al.* at $\phi_{bulk} = 0.30$ and $R_0/a = 17.9$.

simulation results of Nott & Brady (1994) for the flow of a suspension through a channel similar to those considered here, as well as the available experimental velocity profile measurements for cylindrical tube flows that have been reported by Karnis *et al.* (1966) and Sinton & Chow (1991). For the purpose of comparison with our data, we have rescaled all the reported velocity results so that the area under each profile is equal to the area under a Newtonian profile undergoing two-dimensional channel flow.

For a bulk particle concentration of 0.30, our experimental profiles for a channel gap width to particle diameter ratio of 18 (experiment 562) are compared in figure 11 with the simulation data for a particle areal fraction of 0.45 and $H/a = 18.3$, as well as with the velocity profile results of Karnis *et al.* for a corresponding ratio of tube to particle radius of 17.9. As shown in figure 11(*a*) all three profiles appear blunted and quantitatively similar, with the two sets of experimental velocity data bounding the simulation results. Close agreement is observed between our experimental data and the simulation results, particularly in the region near the channel axis.

Concentration data from experiment 562 are also presented along with the corresponding Stokesian Dynamics simulation result in figure 11(*b*), where for comparison purposes, the original areal fractions from the simulation have been converted to volume fractions (dividing by 1.5), and re-scaled so that the volume flux of particles through their channel was equal to the product of the area under their re-scaled velocity profile and the bulk particle volume fraction, e.g. $4\phi_{bulk}/3$. In general, the agreement between the two profiles is quite good, except for the small regions near the channel walls, where the experimental data are lower than the corresponding

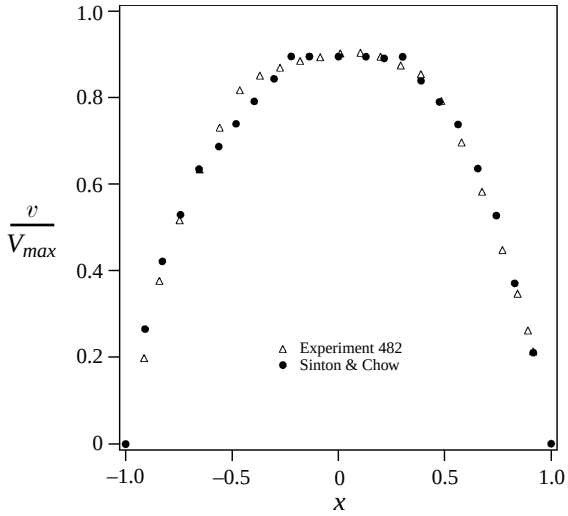

FIGURE 12. Comparison of results at $H/a = 24$ with the velocity data of Sinton & Chow at $\phi_{bulk} = 0.40$.

simulation results. As noted above, the close agreement of these profiles strongly suggests that our measurements were performed at a position sufficiently far downstream from the channel entrance so that the profiles were very close to fully developed.

The assumption of isotropy of the time-averaged squared fluctuational velocity due to viscous particle interactions enables the experimental data for one component of the fluctuational velocity to be extrapolated to three dimensions and compared to the Stokesian Dynamics results for the suspension temperature. This result is presented in figure 11(*c*). Although both data sets are similar in that they possess a minimum at the channel centre and maximum close to the wall, the maximum in the experimental data is lower than that for the simulation. Moreover, the experimental peaks are located closer to the channel wall, which as will be shown in the next section, is in better agreement with numerical results from the Nott & Brady version of the suspension balance model.

At higher concentrations we compare our velocity profile results with the NMR of Sinton and Chow. Although this method measures the velocity of the suspending fluid, we will use our result for the inter-phase slip to assume that the two phases translate with the same velocity distribution across the conduit cross-section. Also, since their data were collected for a suspension flowing through a cylindrical tube for which R_0/a was almost five times the largest H/a incorporated in our experiments, we will take advantage of weak relative channel gap width effects predicted by the suspension balance model and observed in our data, to contrast these results with our result at $H/a = 24$. The plot of figure 12 shows results for $\phi_{bulk} = 0.40$, where close agreement between the two data sets is observed. One intrinsic advantage of the NMR method is also illustrated, which is its ability to elucidate the velocity at a position much closer to the conduit wall.

7. Comparison with model predictions

In this section we test the applicability of the diffusive flux, suspension balance, and Mills & Snabre models introduced in §1 by comparing their predicted results for two-

dimensional channel flow with our experimental data. For all three models, we have calculated steady-state velocity and concentration profiles, and in the case of the suspension balance model, we have also obtained suspension temperature profiles corresponding to each value of ϕ_{bulk} and H/a. In addition to comparing our data with model calculations using parameter values fit by other investigators, we also present results with model parameters set to provide a best fit to our entire set of experimental data.

In §1 it was noted that all three models treat the suspension as a generalized Newtonian fluid with a local particle-concentration-dependent viscosity. In fact, differences in their calculated velocity profiles result from the choice of the empirically derived equation that relates the local viscosity to the local particle concentration, as well as from the different approaches taken to derive equations for the distribution of particles. In any case, a solution for the velocity profile was generated using the appropriate relation over half the channel gap using fourth-order Runge–Kutta numerical integration along with a no-slip boundary condition at the channel wall. This resulting velocity field was then rescaled so that the area under the profile was equivalent to that corresponding to a parabolic profile.

7.1. *Diffusive flux model*

By fitting their NMR wide-gap Couette data to this model, Phillips *et al*. determined that $K_c/K_\mu = 0.66$, and subsequently $\chi \approx 1$, which reduces (1) to the following simple analytical form

$$\phi = \frac{\phi_m}{1+kx}. \tag{23}$$

The constant k of (1) and (23) is found from the constraint on the total flux of particles through the channel

$$\int_0^1 v(x)\,\phi(x)\,\mathrm{d}x = \frac{2\phi_{bulk}}{3}. \tag{24}$$

In addition to the result given by (23), we have found that $\chi = 0.54$ provided a slightly better fit to our experimental velocity data. The solution for the latter case required successive iterations of (1) to calculate the concentration profile, where initial values were provided by (23). Convergence was assumed once the root-mean-square difference between consecutive iterations over the 1000 discretization points was less than 10^{-4}.

Comparison of the results of the model calculations outlined above with our experimental data are presented in figures 13(*a*), 13(*b*), and 13(*c*) for respective ϕ_{bulk} values of 0.30, 0.40, and 0.50. In general, the model predictions for the two values of K_c/K_μ provide close agreement with our velocity data at $\phi_{bulk} = 0.30$, with the agreement becoming progressively worse with increasing ϕ_{bulk}. However, it is clear that the magnitude of the velocity profile mismatch is lessened slightly when $K_c/K_\mu = 0.77$. Nevertheless, the model underpredicts the increased blunting of the velocity profile with increased bulk particle concentration, suggesting the need for a viscosity relationship that is more sensitive to increases in particle concentration. Conversely, better agreement of the model calculations with our concentration data is achieved at higher values of ϕ_{bulk}, particularly within the inner 80% of the channel gap. As noted previously, this latter observation is partially due to the fact that the model predicts a particle concentration equal to ϕ_m at the channel axis for all values of ϕ_{bulk}, which is a consequence of its failure to account for the physical size of the particles.

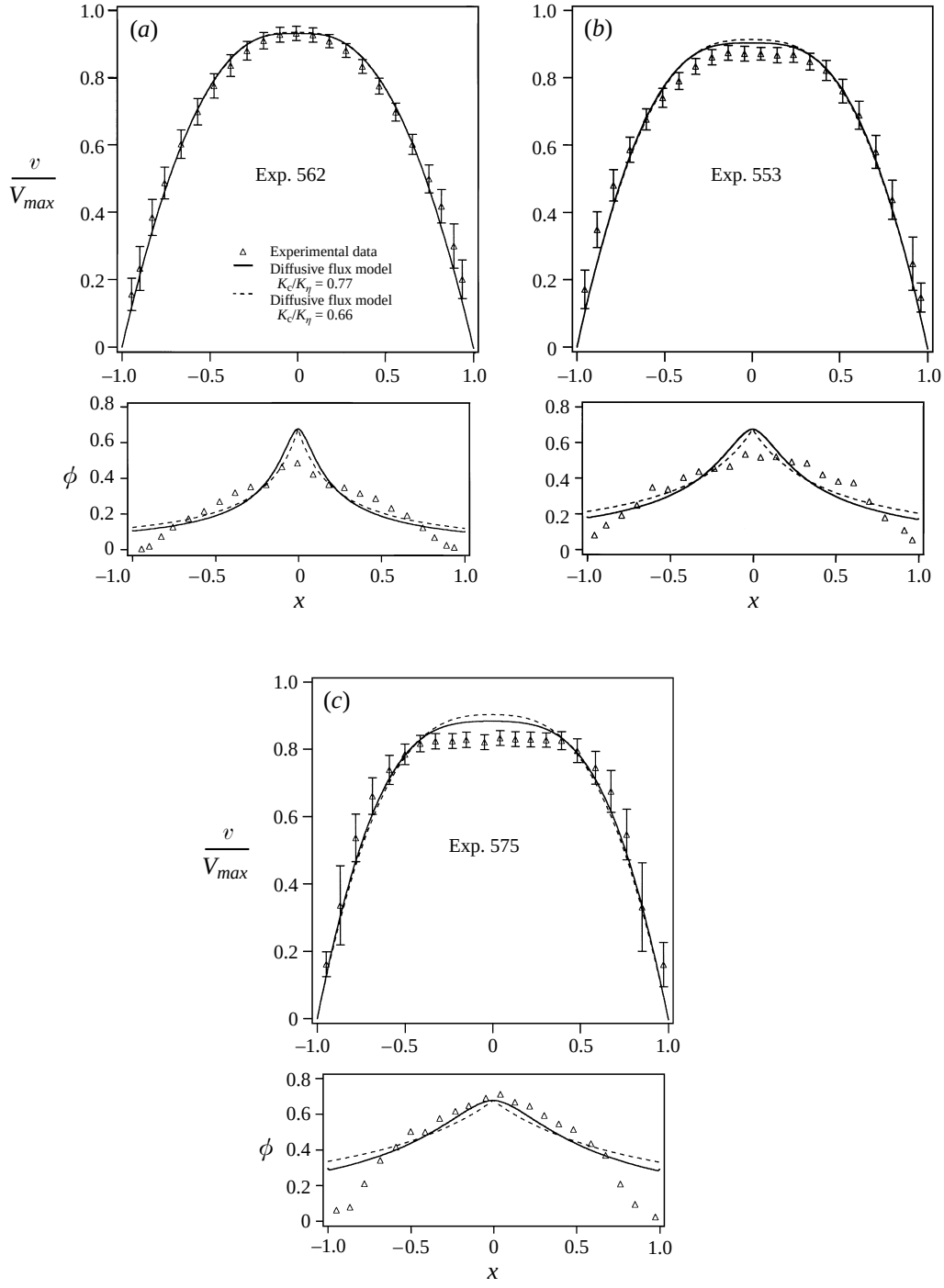

FIGURE 13. Comparison of experimental velocity and concentration profile data with diffusive flux model predictions at (*a*) $\phi_{bulk} = 0.30$, (*b*) $\phi_{bulk} = 0.40$, (*c*) $\phi_{bulk} = 0.50$.

7.2. *Mills & Snabre model*

Owing to the fact that this model produces an analytical result for the concentration profile,

$$\phi = \frac{\phi^*}{1+\alpha x^2}, \tag{25}$$

the solution procedure was identical to that for the diffusive flux model. The empirical viscosity relationship used for this model is that developed by Mills (1985),

$$\frac{\mu(\phi)}{\mu_0} = \frac{(1-\phi)}{(1-\phi/\phi^*)^2}, \tag{26}$$

where $\phi^* = 0.62$ was used.

Results for this model are compared with experimental data at bulk particle concentrations of 0.30, 0.40, and 0.50 and presented in figures 14(*a*), 14(*b*), and 14(*c*). In contrast to the diffusive flux model results, close agreement between the model calculations and the velocity profile data is found for each value of ϕ_{bulk}. The model concentration profiles also show fair agreement with our concentration data, particularly at $\phi_{bulk} = 0.30$ and 0.40, where the calculated profiles tend to provide an average fit to the data points in each figure. It is important to point out that this model also predicts a channel axis concentration of ϕ^* for the same reasons mentioned previously for the diffusive flux model.

7.3. *Suspension balance model*

In implementing this model we have borrowed the conservation equation for the suspension temperature and functional forms for the concentration dependence of the suspension viscosity and particle normal stress developed by Morris & Brady (1998). Boundary conditions required for the velocity, concentration, and temperature profiles include a symmetry condition on the suspension temperature at the channel axis

$$\frac{\mathrm{d}T}{\mathrm{d}x} = 0 \quad \text{at} \quad x = 0, \tag{27}$$

and the particle flux constraint (24). A second boundary condition for the suspension temperature at the wall ($x = 1$) was also necessary to determine the temperature profile. Two semi-empirical conditions have been employed, which balance fluctuational energy produced within the suspension due to shearing at the wall and losses resulting from dissipation of fluctuational velocity by the wall,

$$T = \frac{\mu_p(\phi)}{20\alpha(\phi)}\left(\frac{\mathrm{d}v}{\mathrm{d}x}\right)^2 \quad \text{at} \quad x = 1, \tag{28a}$$

$$T = \frac{\mu_p(\phi)}{\alpha(\phi_w)}\left(\frac{\mathrm{d}v}{\mathrm{d}x}\right)^2 \quad \text{at} \quad x = 1, \tag{28b}$$

The condition (28*a*) is the weak condition of Morris & Brady (1998). For this condition an *ad hoc* constant (equal to 20) multiplies the function that accounts for the particle concentration dependence of the fluctuational velocity dissipation $\alpha(\phi)$, in order to model the confining wall as a suspension at near maximum packing. A similar wall argument is incorporated via the condition (28*b*), where α is evaluated at an *ad hoc* effective confining wall concentration, $\phi_w = 0.675$. Although the chosen form of $\alpha(\phi)$ is sensitive to high particle concentrations, this latter condition is actually weaker than the former, since it results in a larger non-zero wall temperature.

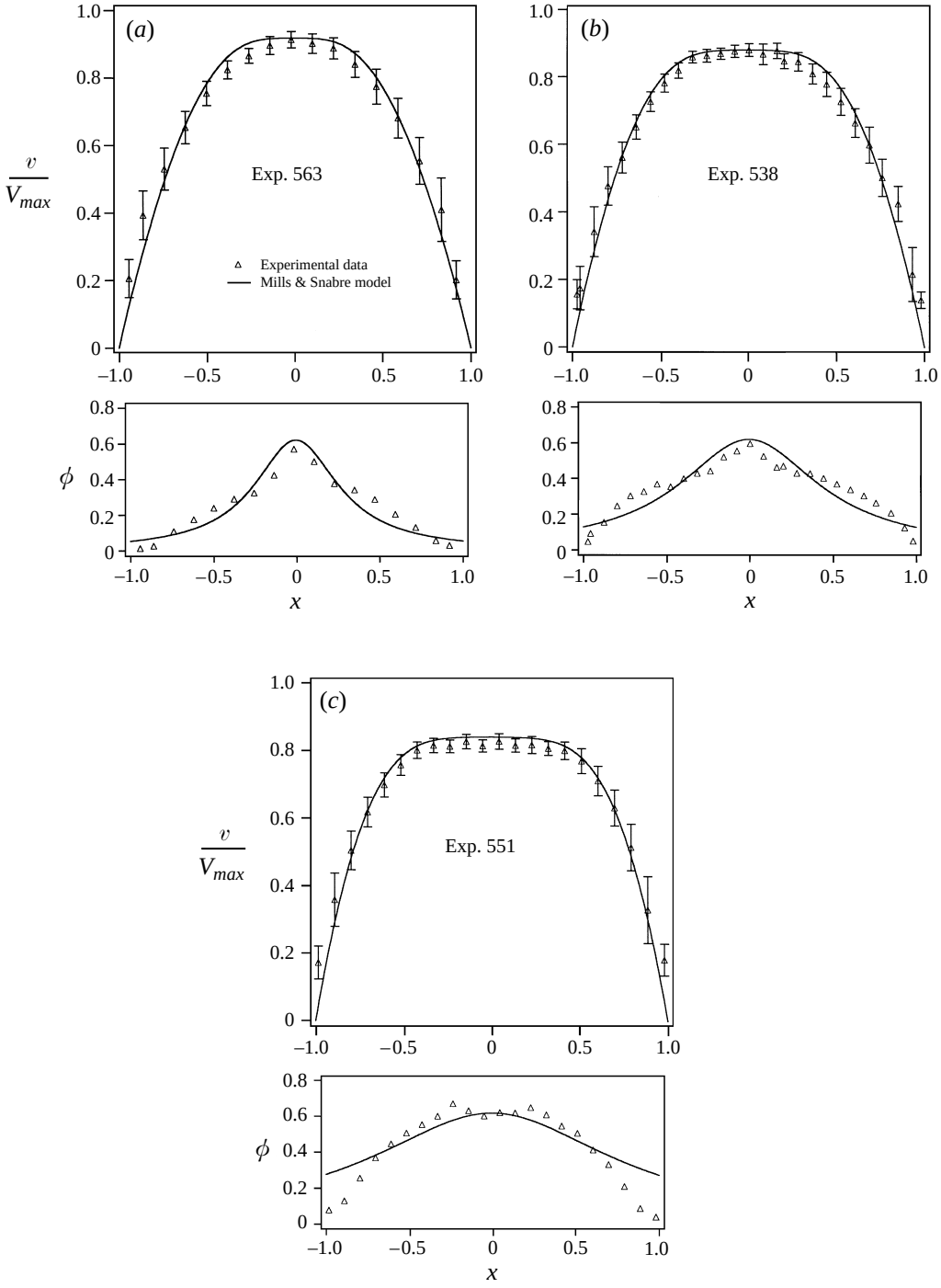

FIGURE 14. Comparison of experimental velocity and concentration profile data with Mills & Snabre model predictions (*a*) $\phi_{bulk} = 0.30$, (*b*) $\phi_{bulk} = 0.40$, (*c*) $\phi_{bulk} = 0.50$.

Velocity, concentration, and temperature profiles were calculated using an iterative procedure, where a first guess for the concentration distribution was input into the momentum balance equation, and a solution for the corresponding velocity profile was generated. The resulting velocity and concentration profiles were then input into the conservation equation for the mean-square particle velocity fluctuation, which had been discretized over half the channel gap using central difference approximations. The corresponding temperature distribution was then calculated via implicit numerical integration. This was then used to find the next guess for the concentration distribution, with the constant of integration being evaluated from (24). Convergence was assumed when the average root-mean-square difference between consecutive concentration distributions was less than 10^{-5} for the 1000 nodes points considered.

Two versions of this model were utilized for comparison with our experimental data. The first was that used by Morris & Brady for comparisons with their Stokesian Dynamics simulation results for the case of channel flow of a non-neutrally buoyant suspension. In this form of the model the particle pressure was assumed to result only from fluctuational forces, $w_t = 1$, and the boundary condition (28*a*) was used. Moreover, values for the two fit parameters k_α and k_κ, which scale the relative magnitudes of dissipation and conduction in the fluctuational energy balance, were set to 0.815 and 0.8, respectively. The second version represents a basic fit to the experimental data and utilizes the temperature boundary condition of (28*b*), as well as parameter values of $w_t = 0.3$, $k_\alpha = 0.13$, and $k_\kappa = 100$.

Comparisons of these two versions of the model with our experimental data at corresponding bulk particle concentration and ratio of channel gap width to particle diameter values of 0.30 and 14, 0.40 and 24, and 0.50 and 11, are presented in figure 15. Both model forms provide good agreement with the experimental velocity and concentration data, particularly for the cases at $\phi_{bulk} = 0.30$ and 0.40. Examination of the result for $\phi_{bulk} = 0.50$, shows that the Morris & Brady version underpredicts the blunting of the velocity profile, while our best-fit version of the model provides close agreement. The Morris & Brady calculated concentration profiles also reveal a boundary layer near the walls, which is not as evident in the best-fit profiles due to our choice for the form of the particle pressure. The biggest difference between the two versions of the model, however, is found in the temperature plots. Here we have assumed that the particle fluctuational energy is isotropic, which enables us to multiply our one-dimensional experimental result by three in order to obtain an approximate measure of the suspension temperature. The results show that although both versions of this model predict similar temperatures at the region near the channel axis, the Morris & Brady result underpredicts the near-wall maximum by an approximate factor of three.

8. Summary

In this work we have demonstrated the application of our modified LDV method to measure fully developed particle velocity, concentration, and time-average squared particle velocity fluctuation distributions for concentrated monodisperse suspensions undergoing approximate two-dimensional pressure-driven flow through a rectangular channel. In general we report non-uniform particle concentration distributions, blunted velocity profiles, and non-uniform time-average squared particle velocity fluctuation profiles, which are qualitatively consistent with predictions from the diffusive flux, suspension balance, and Mills and Snabre models. In Part 2 of this series (Lyon & Leal 1998) we apply this same technique to measure overall particulate-phase

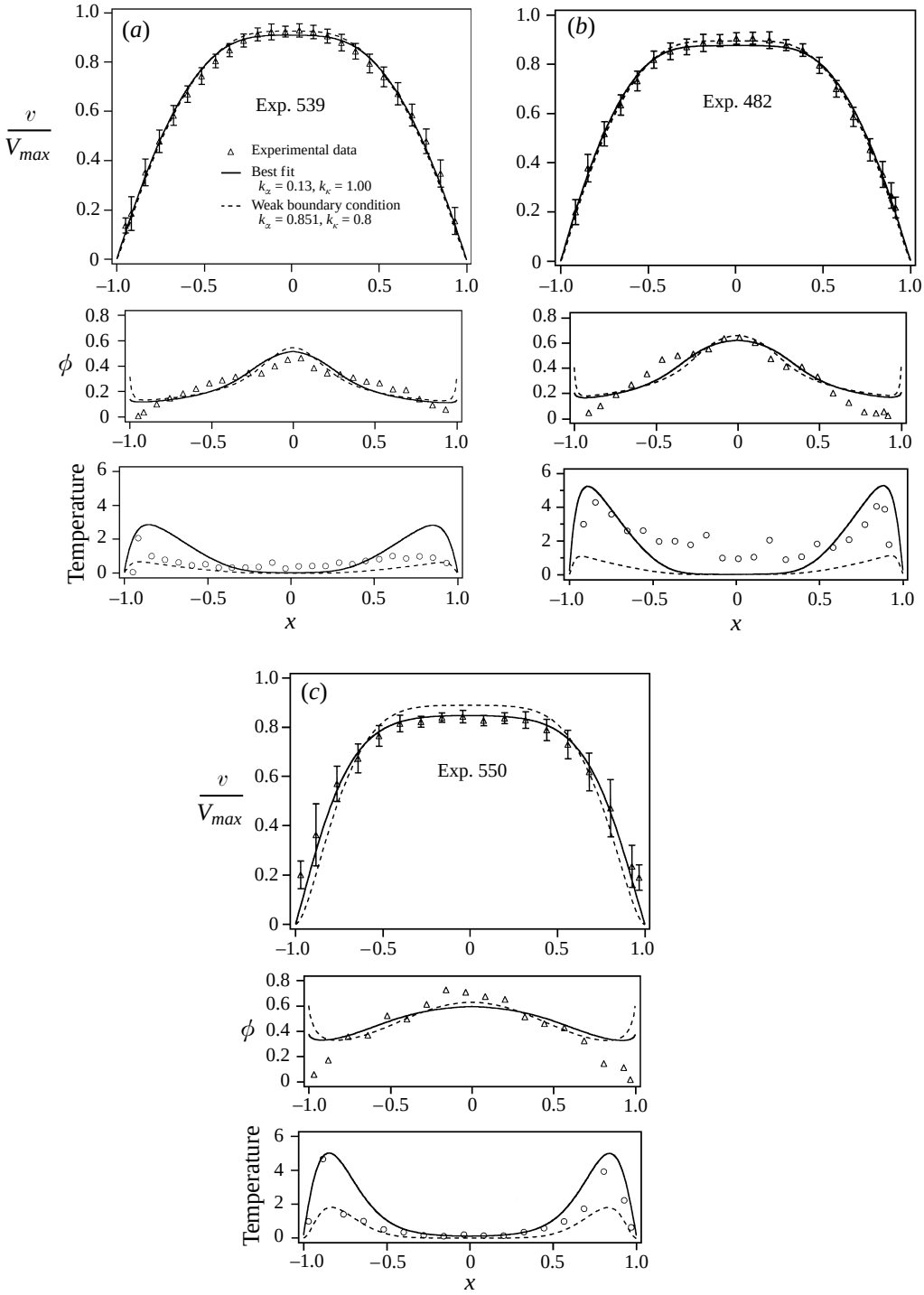

FIGURE 15. Comparison of experimental velocity, concentration, and suspension temperature profile data with suspension balance model predictions for (*a*) $\phi_{bulk} = 0.30$ and $H/a = 14$; (*b*) $\phi_{bulk} = 0.40$ and $H/a = 24$; (*c*) $\phi_{bulk} = 0.50$ and $H/a = 11$.

velocity and concentration profiles for suspensions having a bimodal distribution of particle size.

For a future study it is of interest to obtain experimental data for the evolution of the particle velocity, concentration, and time-average squared particle velocity fluctuation profiles under flow conditions similar to those considered in this work. The acquisition of these data is significant, since it would allow quantitative determination of the evolutionary state of results already present within the research literature, and more importantly, could be used to further test the quantitative applicability of the current models. Although we have attempted such a study within our lab, we were unable to obtain a uniform particle concentration distribution and parabolic velocity profile near the entrance of our channel. However, we have found that a perturbed non-fully developed concentration distribution does evolve toward a fully developed concentration profile over a channel length that scales as $(H/a)^2$ (Lyon 1997), which is consistent with the numerical results of Phan-Thien & Zang (1996) for the perturbation of a fully developed concentration profile.

REFERENCES

Abbott, J. R. & Tetlow, N. 1991 Experimental observations of particle migration in concentrated suspensions: Couette flow. *J. Rheol.* **35**, 773–795.

Adrian, R. J. 1980 *Laser Velocimetry*. University of Illinois, Urbana-Champaign.

Altobelli, S. A. & Givler, R. C. 1991 Velocity and concentration measurements of suspensions by nuclear magnetic resonance imaging. *J. Rheol.* **35**, 721–734.

Atkinson, C. M. & Kytomaa, H. K. 1993 Acoustic properties of solid-liquid mixtures and the limits of ultrasound diagnostics-I: Experiments. *Trans. ASME: J. Fluids Enging* **115**, 665–675.

Averbakh, A., Shauly, A., Nir, A. & Semiat, R. 1997 Slow viscous flows of highly concentrated suspensions – Part I: Laser-Doppler velocimetry in rectangular ducts. *Intl J. Multiphase Flow* **23**, 409–424.

Bacri, J.-C. & Hoyos, M. 1991 Ultrasonic diagnostic in porous media and suspensions. *J. Phys. Paris* III **1**, 1455–1466.

Buyevich, Y. A. 1996 Particle distribution in suspension shear flow. *Chem. Engng Sci.* **51**, 635–647.

Chapman, B. 1990 Shear induced migration phenomena in concentrated suspensions. PhD thesis, University of Notre Dame.

Chung, E. Y.-C. 1980 Experimental investigations of the transport properties of flow suspensions. PhD thesis, California Institute of Technology.

Corbett, A. M. & Phillips, R. J. 1995 Magnetic resonance imaging of concentration and velocity profiles of pure fluids and solid suspensions in rotating geometries. *J. Rheol.* **39**, 907–924.

Ding, J. & Lyczkowski, R. W. 1993 Numerical analysis of liquid-solids suspension velocities and concentrations obtained by NMR imaging. *Powder Technol.* **77**, 301–312.

Goldsmith, H. L. & Mason, S. G. 1967 The microrheology of dispersions. In *Rheology Theory and Applications* (ed. F. R. Eirich), vol. 4, pp. 86–246. Academic.

Graham, A. L. & Altobelli, S. A. 1991 NMR imaging of shear-induced diffusion and structure in concentrated suspensions. *J. Rheol.* **35**, 191–201.

Hampton, R. E. & Mammoli, A. A. 1997 Migration of particles undergoing pressure driven flow in a circular conduit. *J. Rheol.* **41**, 621–640.

Hookham, P. A. 1986 Concentration and velocity measurements in suspensions flowing through a rectangular channel. PhD thesis, California Institute of Technology.

Jana, S. C. & Kapoor, B. 1995 Apparent wall slip velocity coefficients in concentrated suspensions of noncolloidal particles. *J. Rheol.* **39**, 1123–1132.

Kapoor, B. & Acrivos, A. 1995 Sedimentation and sediment flow in settling tanks with inclined walls. *J. Fluid Mech.* **290**, 39–66.

Karnis, A. & Goldsmith, H. L. 1966 The kinetics of flowing dispersions I. Concentrated suspensions of rigid particles. *J. Colloid Interface Sci.* **22**, 531–553.

Koh, C. J. 1991 Experimental and theoretical studies on two-phase flows. PhD thesis, California Institute of Technology.

Koh, C. J. & Hookham, P. 1994 An experimental investigation of concentrated suspension flows in a rectangular channel. *J. Fluid Mech.* **266**, 1–32.

Kowalweski, T. A. 1980 Velocity profiles of suspension flowing through a tube. *Arch. Mech.* **32**, 857–865.

Kytomaa, H. K. & Corrington, S. W. 1994 Ultrasonic imaging velocimetry of transient liquefaction of cohesionless particulate media. *Intl. J. Multiphase Flow* **20**, 915–926.

Leighton, D. T. 1985 The shear induced migration of particulates in concentrated suspensions. PhD thesis, Stanford University.

Leighton, D. & Acrivos, A. 1987 The shear-induced migration of particles in concentrated suspensions. *J. Fluid Mech.* **181**, 415–439.

Leighton, D. & Rampall, I. 1993 Measurement of the shear-induced microstructure of concentrated suspensions of noncolloidal spheres. In *Particulate Two-Phase Flow* (ed. M. C. Roco), pp. 190–209. Butterworth-Heinemann.

Lyon, M. K. 1997 Experimental studies of noncolloidal suspensions undergoing two-dimensional flow. PhD thesis, University of California, Santa Barbara

Lyon, M. K. & Leal, L. G. 1998 An experimental study of the motion of concentrated suspensions in two-dimensional channel flow. Part 2. Bidisperse Systems. *J. Fluid Mech.* **363**, 57–77.

Matin, J. & Rakotomalala, N. 1995 Hydrodynamic dispersion of noncolloidal suspensions: measurement from Einstein's argument. *Phys. Rev. Lett.* **74**, 1347–1350.

McTigue, D. F. & Jenkins, J. T. 1992 Channel flow of a concentrated suspension. In *Advances in Micromechanics of Granular Materials* (ed. H. H. Shen, M. Satake, M. Mehrabadi, C. S. Chang & C. S. Campbell), pp. 381–481. Elsevier Science.

Mills, P. 1985 Non-Newtonian behavior of flocculated suspensions. *J. Phys. Lett. Paris* **46**, 301–309.

Mills, P. & Snabre, P. 1995 Rheology and structure of concentrated suspensions of hard spheres, shear induced particle migration. *J. Phys. Paris* II **5**, 1597–1608.

Model IFA 655 Digital Burst Correlation Instruction Manual. 1995 St. Paul, Minnesota, TSI Incorporated.

Morris, J. F. & Brady, J. F. 1998 Pressure-driven flow of a suspension: buoyancy effects. *Intl J. Multiphase Flow* **24**, 105–130.

Nott, P. R. & Brady, J. F. 1994 Pressure-driven flow of suspensions: simulation and theory. *J. Fluid Mech.* **275**, 157–199.

Phan-Thien, N. & Fang, Z. 1996 Entrance length and pulsatile flows of a model concentrated suspension. *J. Rheol.* **40**, 521–529.

Phan-Thien, N. & Fang, Z. 1996 Stability of some shear flows for concentrated suspensions. *Rheol. Acta* **35**, 35–69.

Phillips, R. J. & Armstrong, R. C. 1992 A constitutive equation for concentrated suspensions that accounts for shear-induced particle migration. *Phys. Fluids* A **4**, 30–39.

Seshadri, V. & Sutera, S. P. 1968 Concentration changes of suspensions of rigid spheres flowing through tubes. *J. Colloid Interface Sci.* **27**, 101–110.

Sinton, S. W. & Chow, A. W. 1991 NMR flow imaging of fluids and solid suspensions in Poiseuille flow. *J. Rheol.* **35**, 735–772.